

Cooking Inspired Tough, Adhesive, and Low-temperature Tolerant Gluten-based Organohydrogels for High Performance Strain Sensors

Hang Xu^{a,b}, Xuya Jiang^{a,b}, Xiangsheng Han^{a,b*}, Hongzhen Cai^{a,b*}, Feng Gao^c

^aSchool of Agricultural Engineering and Food Science, Shandong University of Technology, Zibo, 255000, China

^bShandong Research Center of Engineering and Technology for Clean Energy, Zibo, 255000, China

^cZibo Energy Research Institute, Zibo, 255000, China

*Corresponding author. E-mail address: hanxs@sdut.edu.cn (X. Han); chzh@sdut.edu.cn (H. Cai)

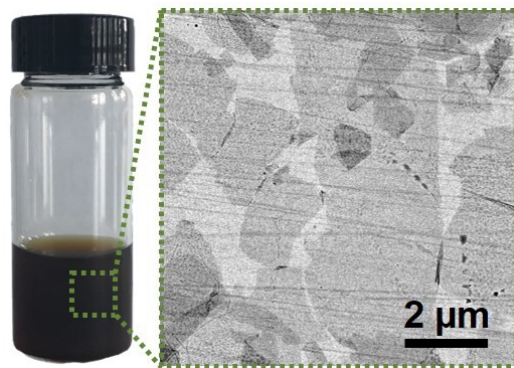


Figure S1. Photograph of GO dispersion and TEM image of GO nanosheets.

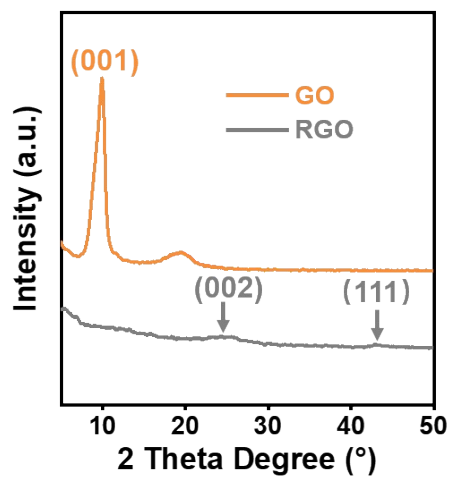


Figure S2. The XRD patterns of GO and RGO.

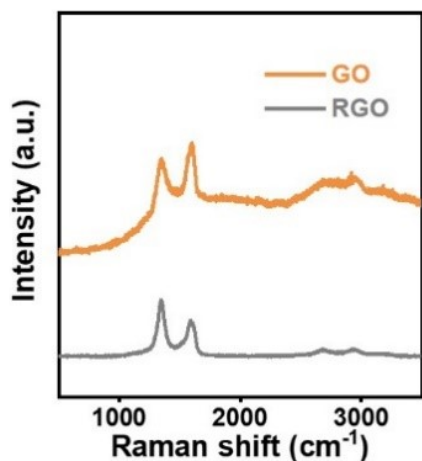


Figure S3. The Raman spectra of GO and RGO. The intensity ratio of I_D/I_G increased from 0.92 of GO to 1.75 of RGO, which was ascribed to the removal of oxygen-containing group of GO and indicated the successful reduction of GO into RGO.

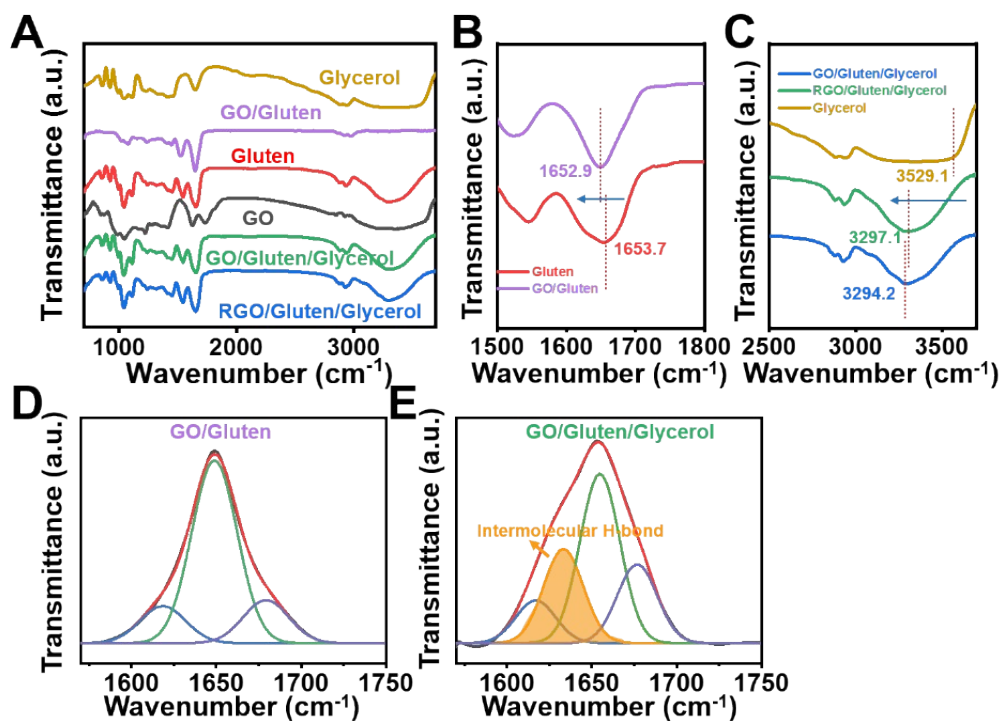


Figure S4. (A) The FTIR spectra of GO, Gluten, Glycerol, GO/Gluten, GO/Gluten/Glycerol, and RGO/Gluten/Glycerol. (B-C) Magnified FT-IR spectra in the range of (B) 1500-1800 cm^{-1} and (C) 2500-3700 cm^{-1} . (D-E) The fitted FT-IR spectra of GO/Gluten and GO/Gluten/Glycerol.

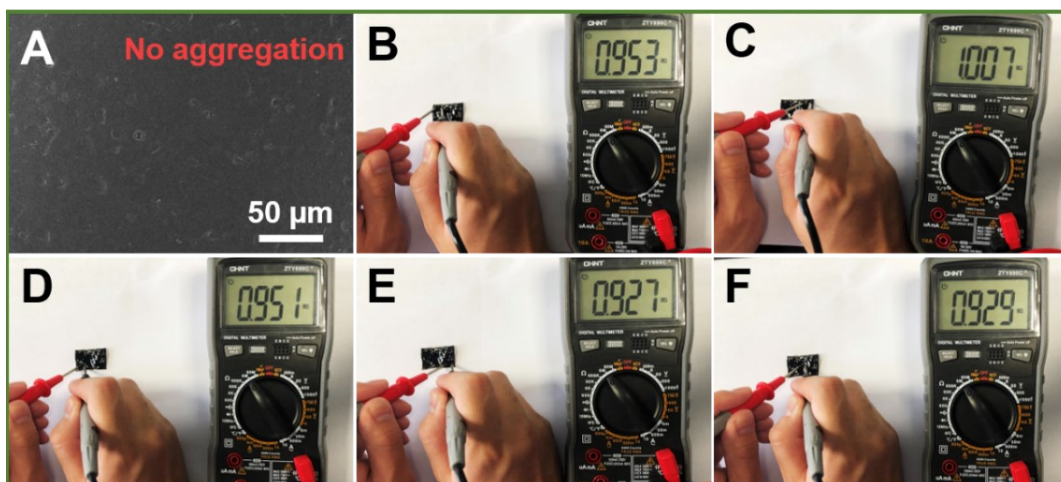


Figure S5. (A) The low-magnification SEM image of GGOH_{0.2}. (B-F) The conductivities of GGOH_{0.2} at different areas indicating the uniform dispersion of RGO in organohydrogels.

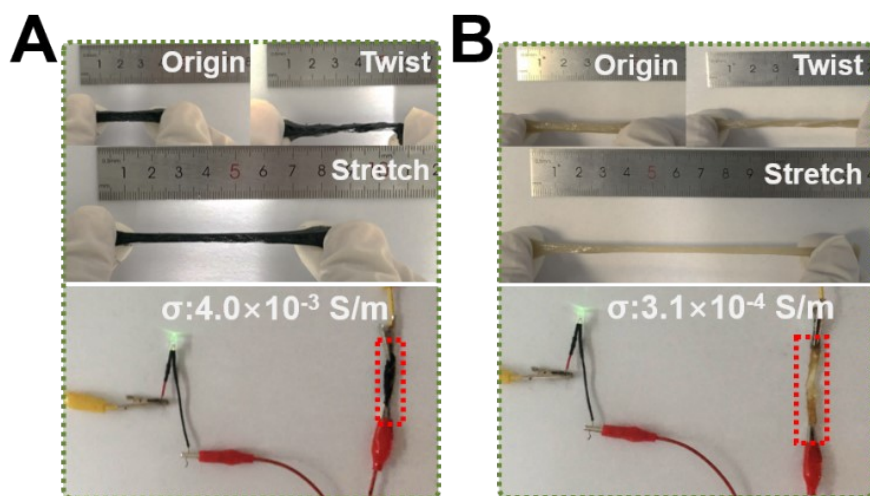


Figure S6. (A-B) The photographs of original, twisting, stretching, and conductive (A) gluten/carbon nanotubes/glycerol and (B) gluten/silver nanowires/glycerol composite organohydrogels.

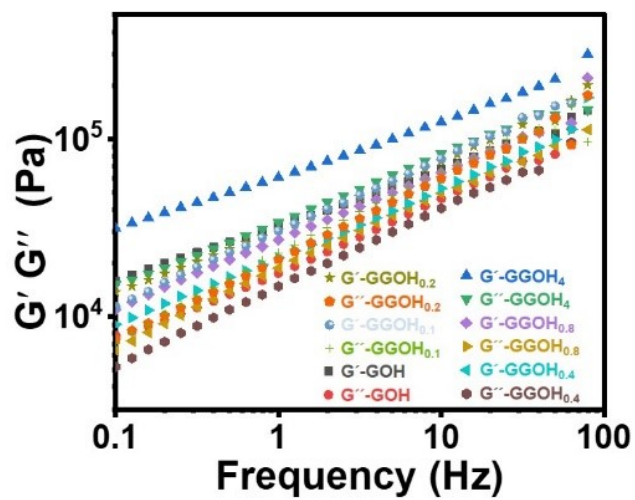


Figure S7. The storage modulus and loss modulus *versus* frequency for the GGOH_x organohydrogels with different RGO concentrations.

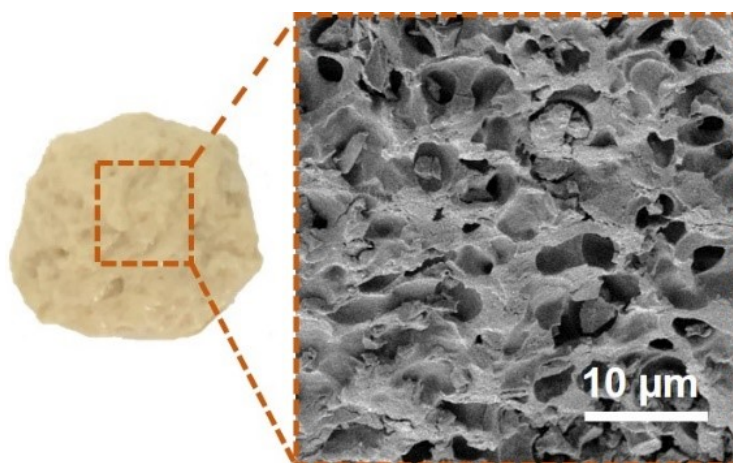


Figure S8. The photograph and SEM image of pure gluten derived from wheat flour dough.

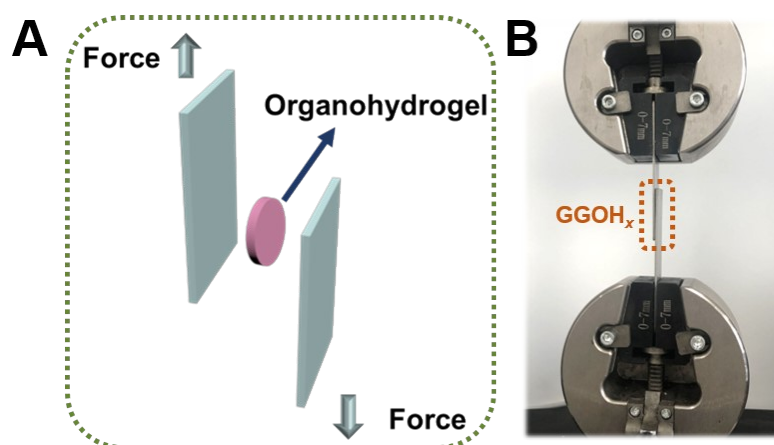


Figure S9. (A-B) Schematic illustration and photograph of the lap-shear measurement.

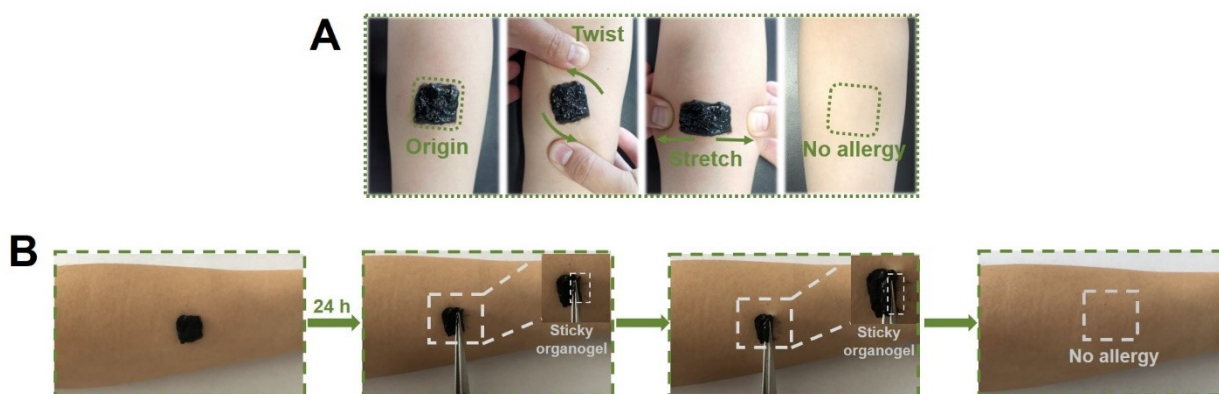


Figure S10. (A) Photographs of GGOH_{0.2} adhered on human skin indicating the tight and comfortable adhesion. (B)

Photographs of GGOH_{0.2} adhered on human skin after 24 h indicating the stable and comfortable adhesion.

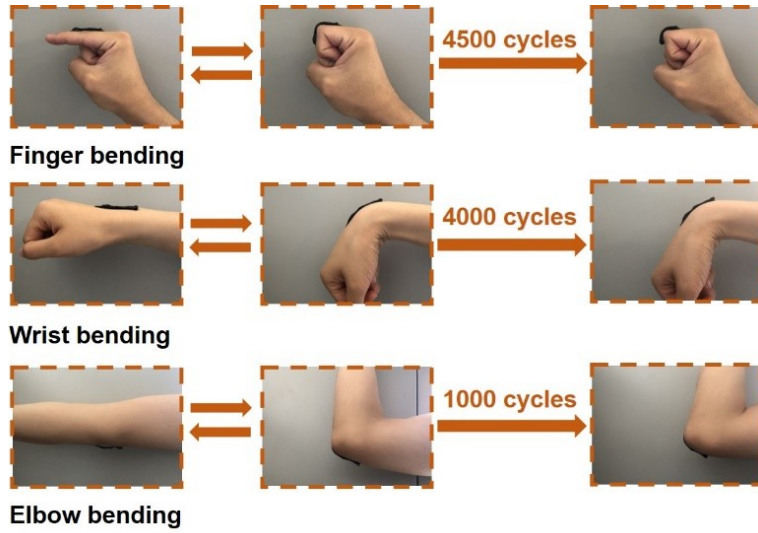


Figure S11. The photographs indicating tight adhesion and anti-fatigue capabilities of GGOH_{0.2} under different human joints bending cycles.

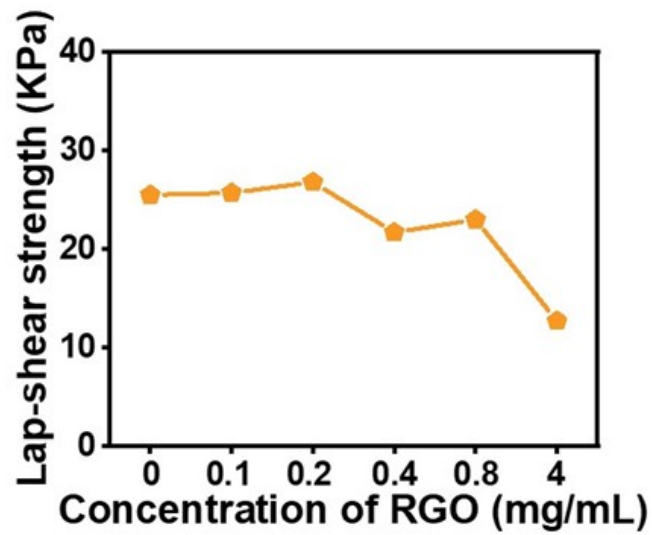


Figure S12. The lap-shear strengths of GGOH_x with different RGO concentrations.

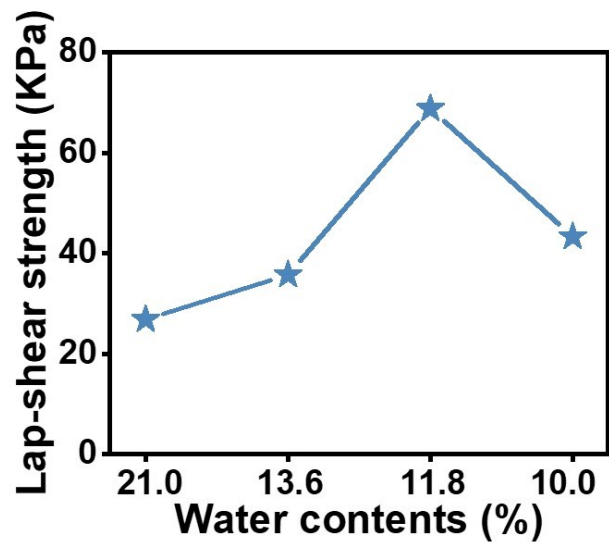


Figure S13. The lap-shear strengths of GGOH_{0.2} with various water contents.

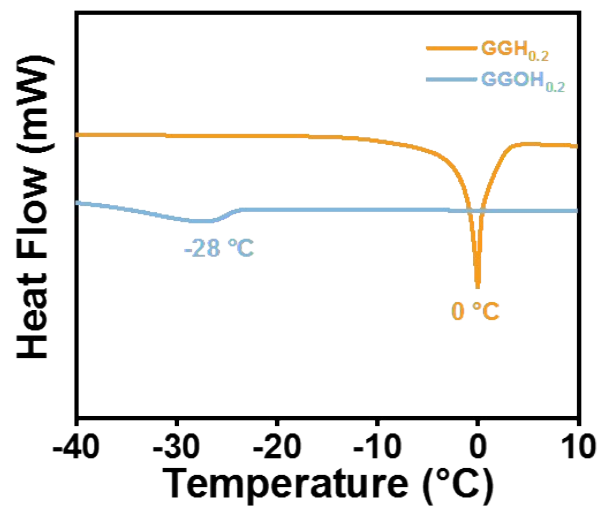


Figure S14. DSC curves of GGOH_{0.2} (with glycerol) and GGH_{0.2} (without glycerol).

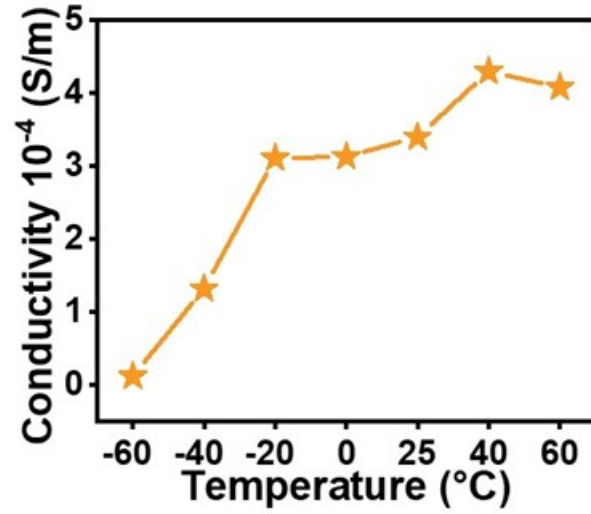


Figure S15. The conductivities of GGOH_{0.2} versus temperature ranging from -60 °C to 60 °C.

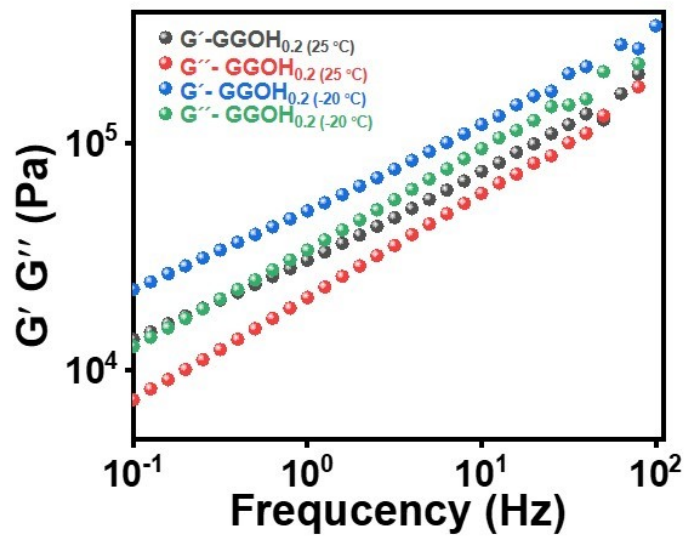


Figure S16. The storage modulus and loss modulus of GGOH_{0.2} under -20 °C and 25 °C.

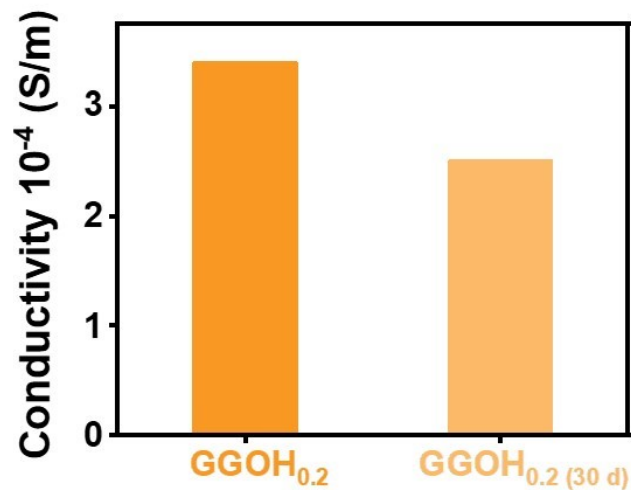


Figure S17. The conductivities of GGOH_{0.2} before and after storing at 25°C and a relative humidity of ~65 % for 30 days.

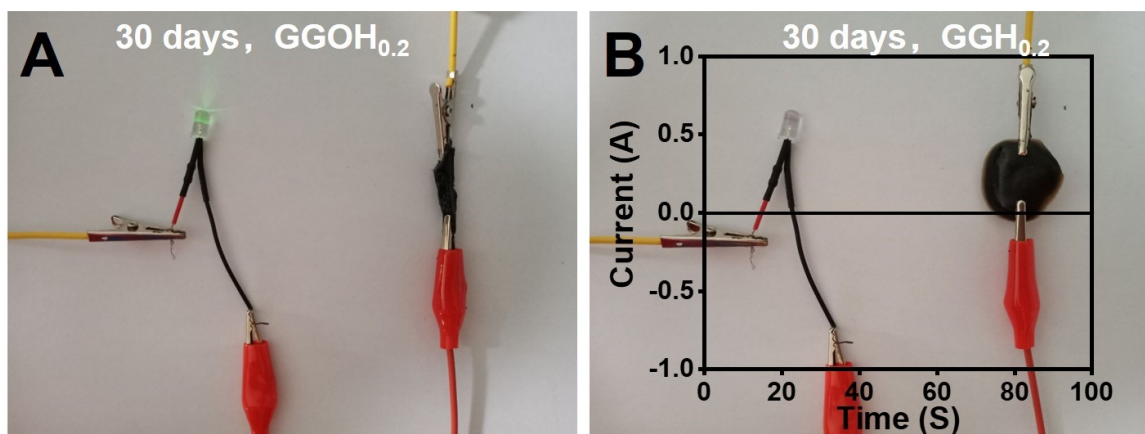


Figure S18. (A-B) Circuits consisting of a green LED indicator and GGOH_{0.2} or GGH_{0.2} that stored at 25°C and a relative humidity of ~65 % for 30 days.

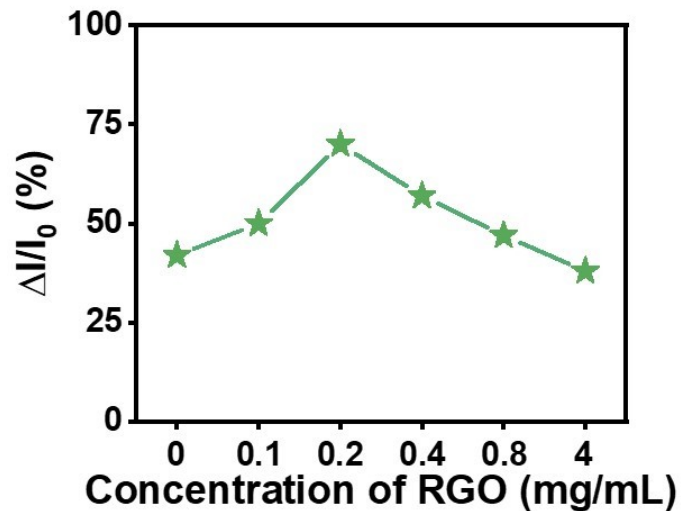


Figure S19. The current variations of $GGOH_x$ at a strain of 80 % with different RGO concentrations.

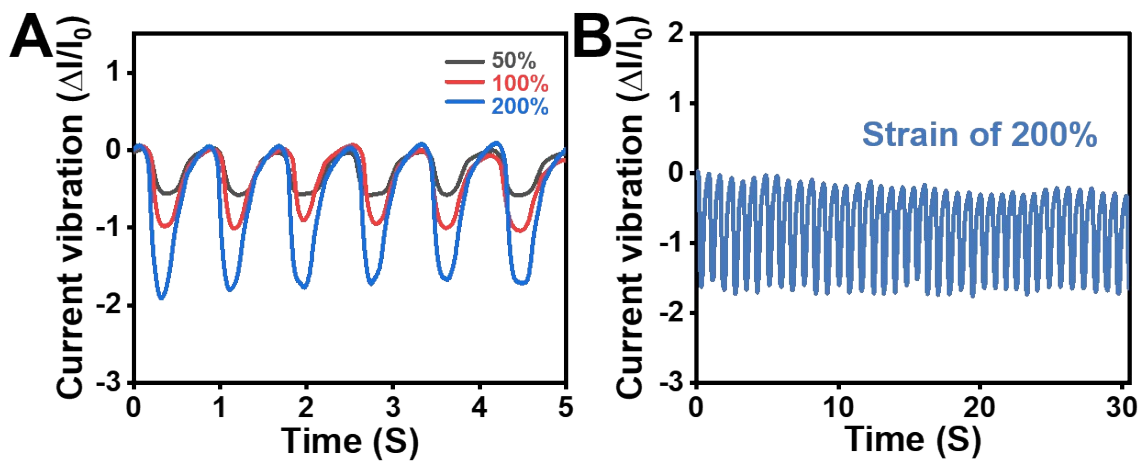


Figure S20. (A-B) Multi-cycle tests of relative current variation of the assembled $GGOH_{0.2}$ strain sensors under strains of 50 %, 100 %, and 200 %.

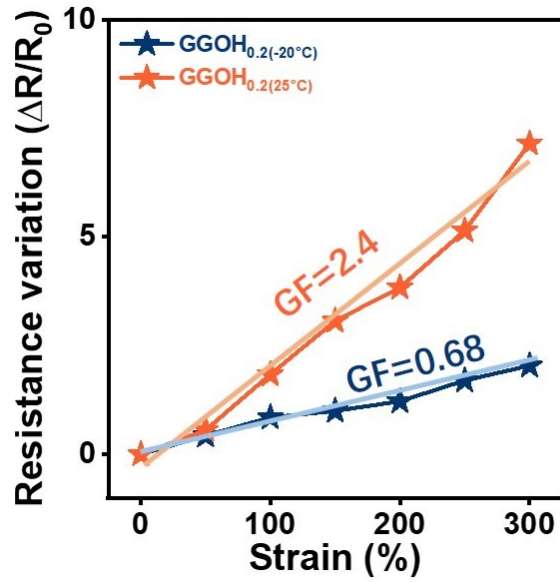


Figure S21. Resistance variations of $GGOH_{0.2}$ versus strains under $-20^\circ C$ and $25^\circ C$.

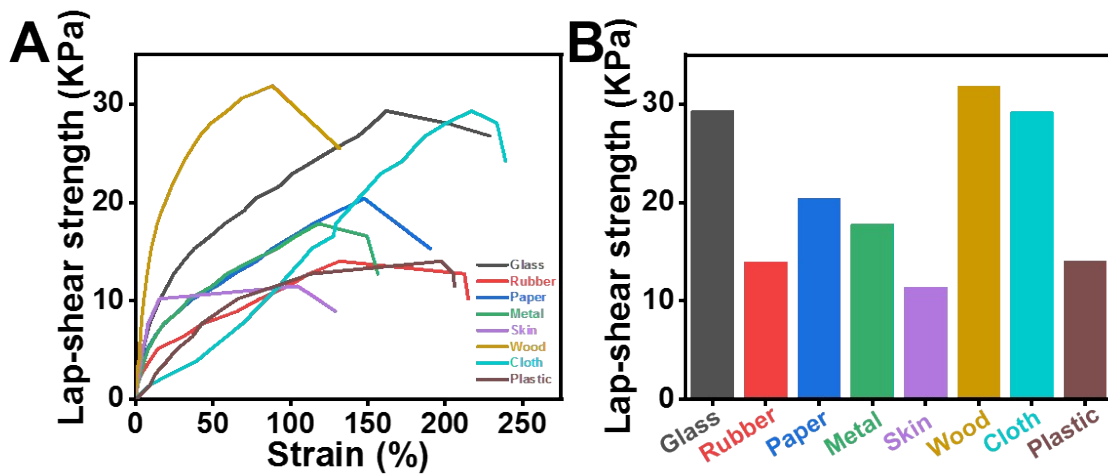


Figure S22. (A-B) Representative curves of lap-shear strengths versus strain for $GGOH_{0.2}$ with different substrates (glass, rubber, paper, metal, skin, wood, cloth, and plastic) under $-20^\circ C$.

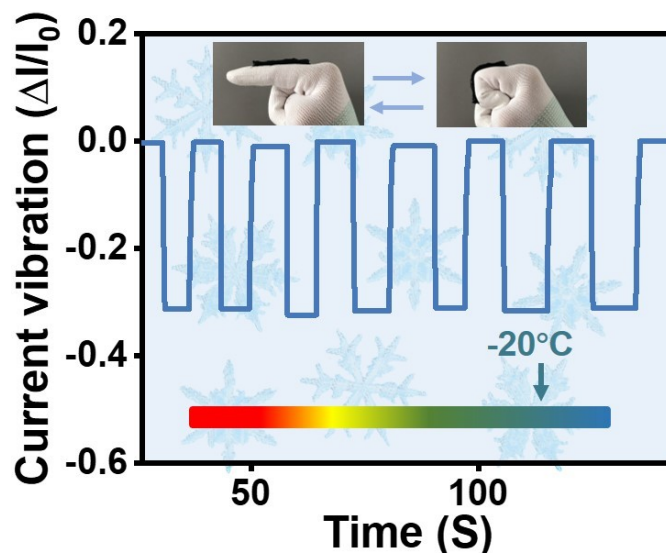


Figure S23. Cyclic tests on the detection of finger bending at a bending angle of 90° under -20°C .

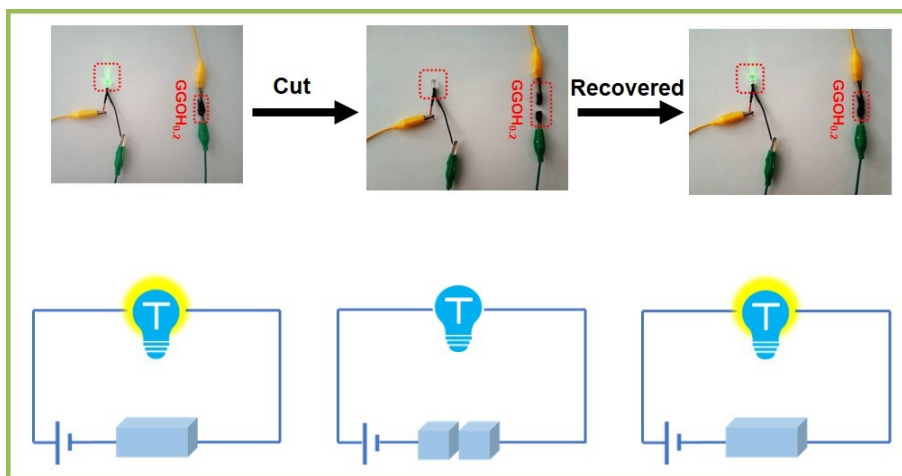


Figure S24. Circuits consisting of a green LED indicator and original $\text{GGOH}_{0.2}$, cut $\text{GGOH}_{0.2}$, and self-recovered $\text{GGOH}_{0.2}$. The corresponding schematic diagrams of these circuits also provided.

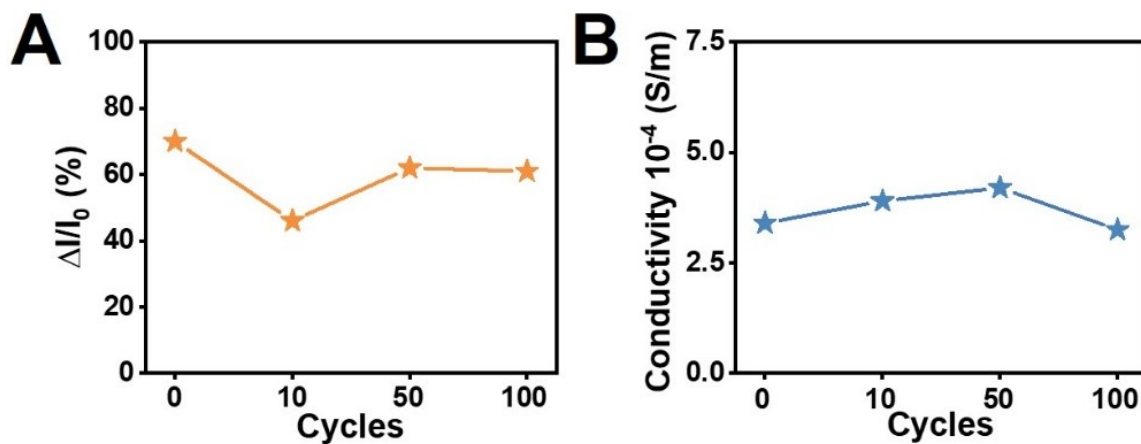


Figure S25. The changes of current variations at a strain of 80 % (A) and conductivities (B) of GGOH_{0.2} after different self-recovery cycles.

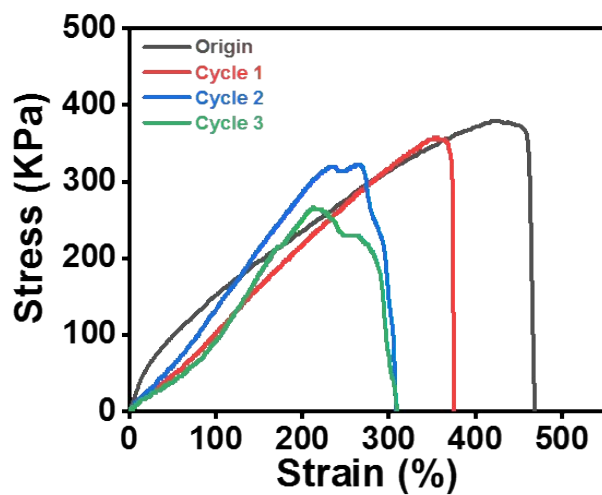


Figure S26. Typical stress-strain curves of GGOH_{0.2} under different cutting-healing cycles.

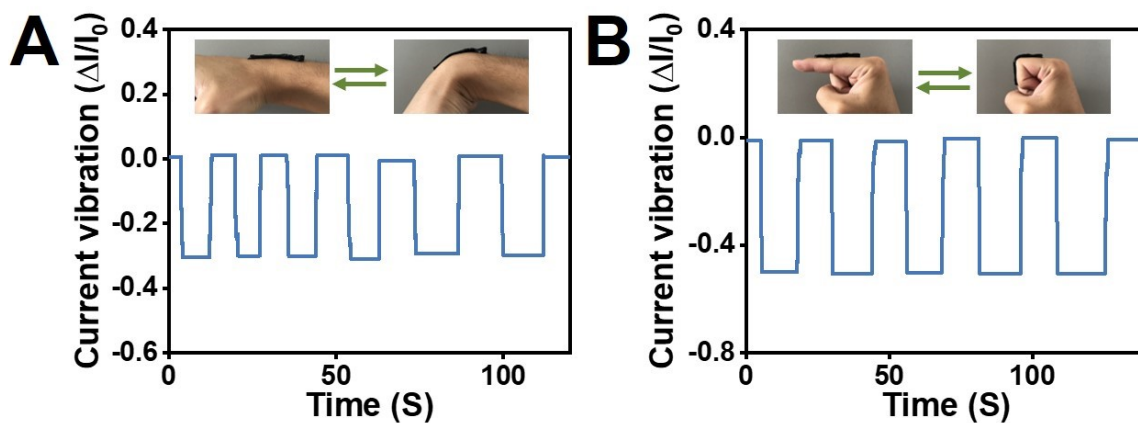


Figure S27. The detection of wrist (A) and finger (B) bending using GGOH_{0.2} after 100 cutting-recovery cycles.

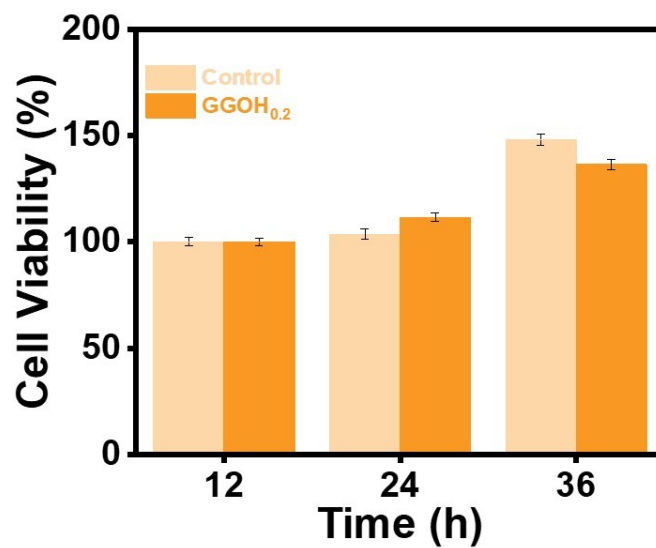


Figure S28. Cell viability of HepG2 cells after 12 h, 24 h, 36 h incubation with GGOH_{0.2}.



Figure S29. Photographs of the degradation of GGOH_{0.2} immersed in KOH (1 mol/L) solution at different times.

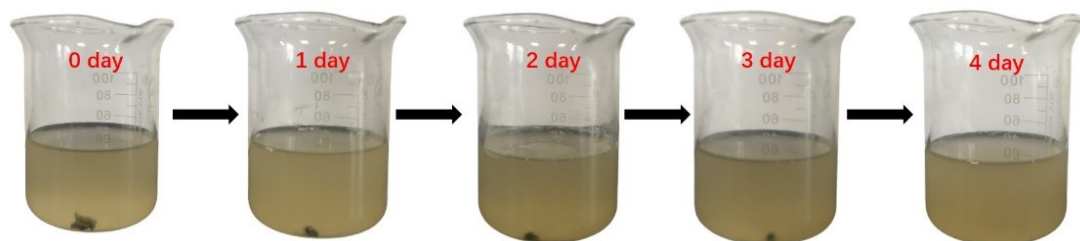


Figure S30. Photographs of the degradation of GGOH_{0.2} immersed in neutral proteinase (5 mg/mL in PBS) solution at different times.

Table S1. The comparison between GGOH_x and some other biomaterials-based hydrogels for the lap-shear strengths

Sample	Lap-shear strength (KPa)	Toughness (MJ/m ³)	Reference
Gelatin/PAA	26.8	0.24	1
CNF/PAM/PDA	28.1	1.80	2
Lignin/PVA/borax	18.7	0.25	3
CNF/PVA/PAM	9.6	0.35	4
CNS/PAM/Ag	17.9	0.96	5
PDA/PVA/graphene	22.0	0.20	6
Bentonite/PDA	23.4	1.75	7
Chitosan/PF127-CHO	6.0	0.008	8
Cellulose/P(DOPMAM-co-MPTC)	25.0	0.02	9
DNA/PEGDA	9.0	0.10	10
Chitosan/PAM	70.0	0.60	11
PDA/CNTs	60.0	0.18	12
GGOH_{0.1}	53.7	1.07	This work
GGOH_{0.2}	68.8	1.14	This work
GGOH_{0.4}	49.8	1.83	This work

and toughness.

References:

1. Z. He and W. Yuan, *ACS Appl. Mater. Inter.*, 2021, **13**, 1474-1485.
2. Z. Shao, X. Hu, W. Cheng, Y. Zhao, J. Hou, M. Wu, D. Xue and Y. Wang, *Nanoscale*, 2020, **12**, 18771-18781.
3. Q. Wang, X. Pan, J. Guo, L. Huang, L. Chen, X. Ma, S. Cao and Y. Ni, *Chem. Eng. J.*, 2021, **414**, 128903.
4. Z. Jin, H. Zhou, J. Lai, X. Jin, H. Liu, P. Wu, W. Chen and A. Ma, *ACS Applied Polymer Materials*, 2021, **3**, 2732-2741.
5. S. Hao, C. Shao, L. Meng, C. Cui, F. Xu and J. Yang, *ACS Appl. Mater. Inter.*, 2020, **12**, 56509-56521.
6. L. Fan, J. Xie, Y. Zheng, D. Wei, D. Yao, J. Zhang and T. Zhang, *ACS Appl. Mater. Inter.*, 2020, **12**, 22225-22236.
7. L. Wu, L. Li, M. Qu, H. Wang and Y. Bin, *ACS Applied Polymer Materials*, 2020, **2**, 3094-3106.
8. J. Qu, X. Zhao, Y. Liang, T. Zhang, P. X. Ma and B. Guo, *Biomaterials*, 2018, **183**, 185-199.
9. S. Lu, X. Zhang, Z. Tang, H. Xiao, M. Zhang, K. Liu, L. Chen, L. Huang, Y. Ni and H. Wu, *Chem. Eng. J.*, 2021, **417**, 129329.
10. D. Wang, J. Cui, M. Gan, Z. Xue, J. Wang, P. Liu, Y. Hu, Y. Pardo, S. Hamada and D. Yang, *Journal of the American Chemical Society*, 2020, **142**, 10114-10124.
11. Y. Cai, J. Qin, W. Li, A. Tyagi, Z. Liu, M. D. Hossain, H. Chen, J.-K. Kim, H. Liu and M. Zhuang, *J. Mater. Chem. A*, 2019, **7**, 27099-27109.
12. L. Han, K. Liu, M. Wang, K. Wang, L. Fang, H. Chen, J. Zhou and X. Lu, *Adv. Funct. Mater.*, 2018, **28**, 1704195.